Structural and electronic modification of photovoltaic SnS by alloying

Citation	Vidal, J., Lany, S., Francis, J., Kokenyesi, R., & Tate, J. (2014). Structural and electronic modification of photovoltaic SnS by alloying. Journal of Applied Physics, 115(11), 113507. doi:10.1063/1.4868974
DOI	10.1063/1.4868974
Publisher	American Institute of Physics Publishing
Version	Version of Record
Citable Link	http://hdl.handle.net/1957/48055
Terms of Use	http://cdss.library.oregonstate.edu/sa-termsofuse

Structural and electronic modification of photovoltaic SnS by alloying

Julien Vidal,[1] Stephan Lany,[1,a)] Jason Francis,[2] Robert Kokenyesi,[3] and Janet Tate[2,b)]
[1]*National Renewable Energy Laboratory, 15013 Denver West Parkway, Golden, Colorado 80401-3305, USA*
[2]*Department of Physics, Oregon State University, Corvallis, Oregon 97331, USA*
[3]*Department of Chemistry, Oregon State University, Corvallis, Oregon 97330, USA*

(Received 8 January 2014; accepted 1 March 2014; published online 19 March 2014)

Emergence of a terawatt scalable photovoltaic (PV) thin film technology is currently impeded by the limited supply of relatively rare elements like In or Te, which has spurred active research in recent years on earth-abundant PV materials. Instead of searching for alternative PV materials, we approach the problem here by structural modification through alloying of a known PV material, namely, tin sulfide. Although SnS is a strong visible light absorber that is naturally p-doped, its indirect band gap reduces the open circuit voltage of SnS-based solar cells. The anisotropic crystal structure results in undesirable anisotropic transport properties. Based on the observation that the isoelectronic sulfides MgS, CaS, and SrS assume the rock-salt structure, we use *ab initio* calculations to explore the structure and electronic properties of metastable $Sn_{1-x}(II)_xS$ (II = Mg, Ca, Sr) alloys, finding that the isotropic rock-salt phase is stabilized above $x = 0.2$–0.3, and predicting direct band gaps in the range of interest for PV applications, i.e., 0.6–1.5 eV for Ca and Sr alloying. We subsequently synthesized such $Sn_{1-x}(Ca)_xS$ films by pulsed laser deposition, confirmed the cubic rock-salt structure, and observed optical band gaps between 1.1 and 1.3 eV. These results highlight the potential of structural modification by alloying as a route to widen the otherwise limited materials base for promising earth-abundant materials. © *2014 AIP Publishing LLC*. [http://dx.doi.org/10.1063/1.4868974]

I. INTRODUCTION

Photovoltaic (PV) technologies based on inorganic thin film absorber materials may enable cost-effective solar energy production at large scales.[1,2] Crystalline Si solar cells are very successful and presently dominate the market, but this technology has intrinsic limitations originating from the strongly indirect band structure character of *c*-Si. In particular, a rather thick absorber layer (typically ~150 μm) with very low defect densities is required, which mandates a fairly complex fabrication process.[3] New successful thin-film materials could lead to a diversification of PV technologies with increased competition and independent supply chains, thereby mitigating the danger of market volatilities. There is increasing concern that the leading thin film technologies, CdTe and $Cu(In,Ga)Se_2$ (CIGS), rely on elements that are toxic (Cd) or rare (Te and In),[4] which has spurred active research in earth-abundant PV materials.[5–8]

During the last few years, SnS has attracted interest as an earth abundant PV absorber that can be grown by a wide range of physical and chemical deposition techniques, in the orthorhombic (orth) structure.[9–12] Besides the need for device optimization, e.g., developing hetero-junction partner materials and contact layers, there are also materials-intrinsic barriers that are related to the anisotropic crystal structure of SnS. First, orth-SnS has an indirect band gap of 1.07 eV (Refs. 9 and 13) and only at energies above about 1.4–1.5 eV is the absorption coefficient is above $10^4\,cm^{-1}$, the value needed for sufficiently complete absorption in a thin film with thickness no more than a few μm.[9] While the indirect band gap character of SnS is much less pronounced than in *c*-Si, where the direct gap lies in the ultraviolet,[14] it nevertheless implies a considerable loss of about 0.3 eV in the achievable open-circuit voltage of a thin-film solar cell. Second, the anisotropic character of the band-structure causes relatively high effective masses for holes in the direction perpendicular to the planes of the layered SnS structure,[9] which reduces the mobility in this direction and is likely to impede the collection of photo-excited carriers.

It appears clear that the drawbacks of SnS as a PV absorber lie in its peculiar crystal structure and that a symmetric phase of SnS is more desirable. The polymorphism of SnS has been investigated to some extent, with various experimental claims having been made about observation of a zinc blende phase,[15,16] a high temperature orthorhombic phase,[17] and a rock salt phase (rs-SnS).[18] rs-SnS is just 40 meV/atom higher in energy than the orthorhombic ground state (orth-SnS).[19] Mariano and Chopra successfully stabilized the rs phase by epitaxial growth on a NaCl substrate.[18]

In this paper, we consider the stabilization of the rs phase by alloying with the sulfides MgS, CaS, and SrS, which assume the rs structure as their ground state. We performed *ab initio* calculations for the alloy mixing enthalpy in either (orth or rs) structure, as well as for the band-structure and optical properties of the rs alloys. Promising properties, i.e., a low mixing enthalpy and a high absorption close to the band gap energy, are predicted for alloys with CaS and SrS. Experimentally, we synthesized $Sn_{1-x}Ca_xS$ alloys by pulsed

a)E-mail: Stephan.lany@nrel.gov
b)E-mail: janet.tate@physics.oregonstate.edu

laser deposition (PLD), confirmed the formation of the isotropic rs structure, and measured optical band gaps in the range of interest for PV applications, i.e., 1.1–1.3 eV.

II. EXPERIMENTAL AND THEORETICAL METHODS

The PLD targets were prepared from mixtures of CaS and Sn metal, with tin to calcium ratios of 2.33:1 and 1:1, which were annealed under flowing H_2S for 4 h at 400 °C. In case of the 1:1 target, the resulting powder was ground, pressed, and then annealed for a further 2 h at 400 °C under flowing H_2S. The 2.33:1 target had approximately 20% excess sulfur added prior to being pressed and annealed in a hot isostatic press (AIP HP630) under Ar. A 248-nm KrF pulsed excimer laser was used for the ablation of the targets. The target-substrate separation was fixed at 5.4 cm. The substrate temperature was varied from 300 to 600 °C with a laser fluence of 1.0 J/cm^2 and pulse rate of 7 Hz. All films were deposited in vacuum, with a base pressure of 10^{-9} Torr. Following deposition, films were cooled rapidly in vacuum.

Glancing incidence x-ray diffraction for phase identification purposes was performed using a Rigaku RAPID diffractometer with an incidence angle of 10°. For lattice parameter measurements, θ-2θ x-ray diffraction patterns were obtained using a Bruker D8 Discover x-ray diffractometer and a Rigaku Ultima IV diffractometer in the parallel beam geometry with Cu K_α radiation. The (200) reflection at $2\theta_{200} = 32.96°$ from the Si substrate was used to calibrate the spectrum. Background subtraction using a polynomial fit was performed, and peaks were fit to a Lorenztian profile to determine the peak positions. Cross sectional imaging and electron diffraction data were obtained using an FEI Titan transmission electron microscope at accelerating voltages of 80 and 200 kV. The samples were rotated to alter the crystallographic direction being measured, and the diffraction from the silicon substrate was used to calibrate the patterns.

The chemical composition of the films was determined by measuring the K_α emission from sulfur, oxygen, silicon, and calcium, and the L_α emission from tin using a Cameca SX 50 electron microprobe at accelerating voltages of 10, 15, and 20 kV. Energy dispersive x-ray spectroscopy was used for stoichiometry measurements of transmission electron microscopy (TEM) samples.

Optical transmission and reflection data were collected using a custom-made spectrometer with a double grating monochromator. Measurements in the ultraviolet and visible regions were performed using a xenon lamp and silicon detector. A tungsten lamp and InGaAs detector were used for near infrared measurements. The absorption coefficient α was calculated using $T/(1-R) = e^{-\alpha d}$, where T is transmission, R is reflection, and d is the film thickness, which was determined using a J.A. Woolam V-VASE spectroscopic ellipsometer. Resistivity and Hall measurements were performed using a LakeShore Cryotronics 7504 Hall effect measurement system at magnetic fields up to 2 T. Electrical contacts were made using pressed indium. Room temperature Seebeck coefficients were measured relative to copper using a custom-built system with a maximum temperature differential across the sample of 5 K.

Ab initio calculations were performed using the VASP package.[20] To compute mixing enthalpy of alloys, we performed density functional theory-generalized gradient approximation (DFT-GGA) total-energy calculations in large supercells of more than 200 atoms. For both the orth and the rs structures, we sampled the alloy concentration by considering several individual random alloy configurations for a given concentration while relaxing both volume and internal coordinates. Band gaps and optical properties were determined from quasiparticle energy calculations within the GW approximation[21] using a fully relaxed 16-atom Special Quasirandom Structure (SQS)[22,23] to simulate the random alloy. The optical spectra were determined from the macroscopic polarizability in the independent particle approximation. Further technical details about the GW calculation can be found in Refs. 9 and 24.

III. ALLOY ENERGETICS, STRUCTURE, AND STABILITY

To explore the possible transition from the orthorhombic structure of SnS into the cubic rs structure, we calculated the mixing enthalpy between SnS and the three group-II sulfides MgS, CaS, and SrS, all of which have the rs phase as the ground state structure. As shown in Fig. 1, the enthalpy of the rs structure becomes lower than that of the orth structure at compositions of $x_{Mg} = 0.23$, $x_{Ca} = 0.18$, or $x_{Sr} = 0.28$, indicating that alloy compositions above these critical values would occur in the cubic phase. The mixing enthalpies of the Ca and Sr alloys are lower than that of the Mg alloy, which is due to the larger lattice mismatch between MgS and SnS. In the cubic rs phase, the calculated lattice constants are 5.22, 5.71, 6.07, and 5.84 Å for MgS, CaS, SrS, and SnS, respectively. Note that within the DFT-GGA approximation used here, lattice constants are generally overestimated by about 1%–2%, compared to experiment.

The mixing enthalpies of the order of 100 meV for the $Sn_{1-x}Ca_xS$ and $Sn_{1-x}Sr_xS$ alloys (see Fig. 1) indicate that there is a miscibility gap under thermodynamic equilibrium conditions, similar to the case of, e.g., the well-studied

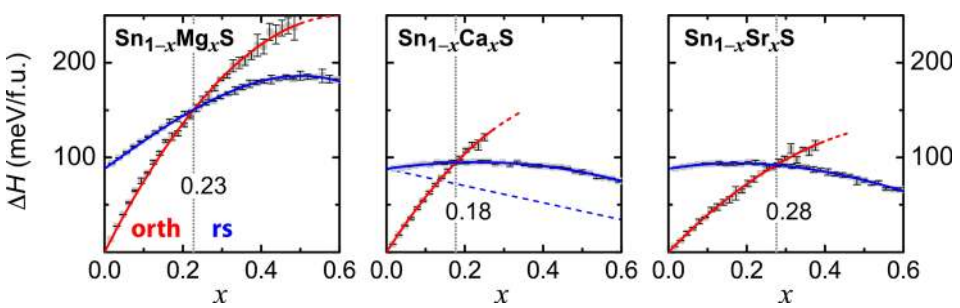

FIG. 1. The calculated mixing enthalpy ΔH per formula unit for $Sn_{1-x}(II)_xS$ alloys (II = Mg, Ca, Sr), showing the transition from orth to rs as the structure with the lowest enthalpy at critical compositions between $0.18 \le x \le 0.28$. The dashed line shown for the Ca alloy is a guide to the eye to illustrate the mixing enthalpy relative to the rs phases of SnS and CaS.

$Ga_{1-x}In_xN$ alloys.[25,26] However, it is also well established that such III-V alloys can be grown over the full composition range, aided by non-equilibrium conditions at lower growth temperatures around 600 °C.[27] In contrast to these III-V systems where the alloy components have the same crystallographic phase, the miscibility gap occurs in the present SnS alloys between two different crystallographic phases, suggesting that there exist additional barriers for phase separation that arise due to the surface energy associated with the nucleation of a phase with a different structures. Therefore, once the alloy assumes the rs structure above the critical composition, a possible phase separation would be expected to proceed within the rs structure until sufficiently large Sn-rich regions are formed that are able to overcome the nucleation energy for the precipitation of the orth structure. As illustrated in Fig. 1 for the case of Ca alloying, the mixing enthalpy with respect to the binary end compounds in their rs structure is smaller than that with respect to the binary end compounds in their ground state structures. It can be described by an alloy interaction parameter $\Omega = 162$ meV within the second order approximation $\Delta H = \Omega x(1-x)$ which is considerably smaller than $\Omega \approx 260$ meV for $Ga_{1-x}In_xN$ alloys.[25,26] Thus, within the constraint given by the structural framework of the rs structure, the driving force for phase separation, e.g., via spinodal decomposition, is not very strong, and the growth of rs structure alloys between SnS and CaS or SrS seems to be sufficiently feasible to attempt thin film growth experiments.

IV. SYNTHESIS OF $Sn_{1-x}Ca_xS$ ALLOYS

Thin films of $Sn_{1-x}Ca_xS$ were prepared by PLD on amorphous SiO_2 and ⟨001⟩-oriented single crystal Si with a 100-nm thermal oxide layer at substrate temperatures between 300 and 600 °C. Electron probe microanalysis and energy dispersive X ray spectroscopy indicate that films grown at 300 and 400 °C have about 10% higher calcium content than that of the PLD target. At 500 °C and above, there is a considerable loss of Sn, leading to high Ca compositions, while still preserving a nearly one-to-one cation-to-anion ratio. The films did not show any measurable oxygen content. However, the presence of some oxygen in the films cannot be ruled out because the films were grown on a thermal oxide. The $Sn_{1-x}Ca_xS$ films were typically 100–150 nm thick. The Ca content was $0.39 < x < 0.91$; films with lower x could not be made from the available (Ca,Sn)S targets. We tried to reduce x by producing alternating (Ca,Sn)S and SnS layers deposited from alloy and pure SnS targets, respectively, and annealing the film to mix the layers. However, we could not be sure that annealing would remove all compositional gradients and the effects of layering, so we discarded this option. We also prepared SnS films from SnS_x targets (no Ca) under similar conditions and with similar thickness.[28]

As shown in Fig. 2, the films appear dense and well-crystallized in TEM. The diffraction patterns from observations along ⟨011⟩ and ⟨111⟩ zone axes are consistent with the cubic rock salt structure and do not correlate with patterns from the orthorhombic SnS structure. Thus, the X-ray diffraction of the $Sn_{1-x}Ca_xS$ films confirms that all measured films adopt the cubic rocksalt structure. Glancing incidence x-ray measurements on a film with composition $Sn_{0.38}Ca_{0.62}S$ are shown in Fig. 1 as an example. The reflections with positions and intensities are consistent with the cubic rock salt structure (Fig. 2 and Table I). Reflections from orthorhombic SnS are not present in the measured spectrum. Similar growths of orthorhombic SnS on silicon always result in highly oriented films with only the (0*k*0) peaks present in the x-ray diffraction pattern, and these were not observed in these $Sn_{1-x}Ca_xS$ films. The (002) and (022) reflections from the cubic $Sn_{1-x}Ca_xS$ are readily observed and were used to determine the lattice parameter of the films, which decreases as the calcium content is increased, i.e., from 0.575 nm for $x = 0.4$ to 0.569 nm for $x = 0.92$ (Fig. 2). The lattice parameters were determined from the TEM for two film compositions, $x = 0.39$ and $x = 0.91$, and were consistent with the lattice parameters measured by X-ray diffraction (see Fig. 2(e)). The linear trend of the measured lattice parameter indicated by the fit line in Fig. 2 suggests that the $Sn_{1-x}Ca_xS$ films form a homogeneous solid solution. The linear interpolation of the experimental literature values[29,30]

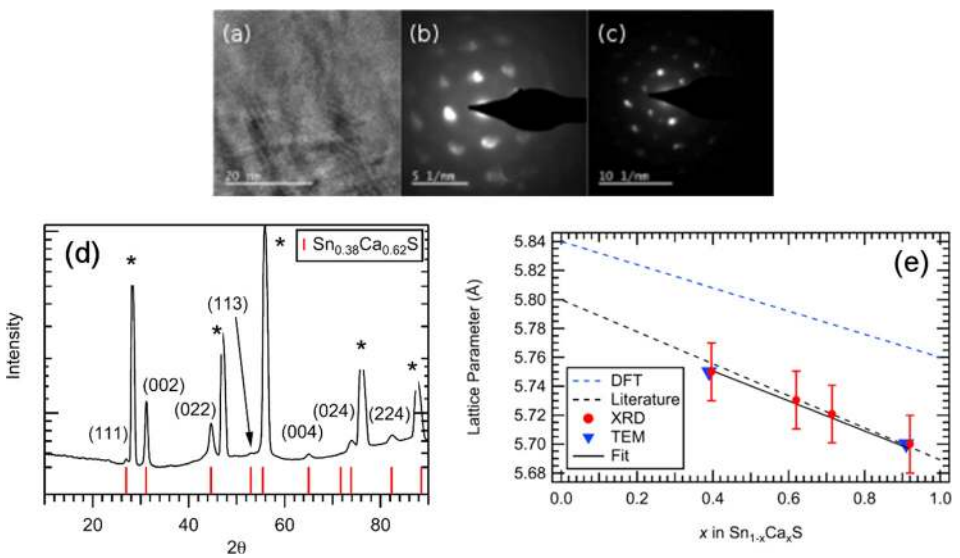

FIG. 2. Structural characterization of $Sn_{1-x}Ca_xS$ thin films: (a) TEM image; (b) and (c) diffraction patterns of along the ⟨001⟩ and ⟨011⟩ zone axes, respectively. (d) Glancing incidence X-ray diffraction (asterisks denote substrate reflections). (e) The lattice parameter as a function of Ca content x. The dashed line is a linear interpolation between the calculated (DFT) and measured (literature) lattice parameters of the binary rs-SnS and CaS compounds.

TABLE I. Calculated peak positions and intensities for cubic $Sn_{0.38}Ca_{0.62}S$ ($a = 0.573$ nm). The intensities for (SnCa)S are weighted averages of intensities of rs-SnS (ICSD-651015) and rs-CaS (ICSD-619534).

	$Sn_{0.38}Ca_{0.62}S$	
(*hkl*)	2 θ	Intensity
(111)	26.93	0.24
(002)	31.19	1.0
(022)	44.69	0.68
(113)	52.95	0.12
(222)	55.50	0.23
(004)	65.05	0.10
(133)	71.74	0.05
(024)	73.91	0.28
(224)	82.38	0.21
(115)	88.61	0.04

for rs-SnS ($a = 0.580$ nm) and CaS ($a = 0.5689$ nm) describes very well the present data for the composition dependence in the alloy. The DFT calculated lattice parameters show a similar relative change between rs-SnS and CaS, the overestimation of the absolute values by about 1% is typical for the generalized gradient approximation.

V. BAND-STRUCTURE AND OPTICAL PROPERTIES OF THE ALLOYS

The optical absorption of orth SnS has been previously studied in detail both experimentally and theoretically.[9–11,13] The indirect band gap lies at 1.07 eV, but the onset of optical absorption in thin films lies somewhat higher around 1.3–1.4 eV due to the indirect and anisotropic nature of the band structure.[10] Complete absorption in a thin film of thickness about 1 μm requires an absorption coefficient above 10^4 cm^{-1}, which occurs only at photon energies above 1.5 eV for SnS. The large difference of 0.4 eV between the band gap and the effective absorption threshold implies considerable loss of efficiency in a solar cell. The goal of the alloying approach is to use the transition from the orth to the rs structure to induce a direct band gap and more isotropic character of the band-structure and optical properties.

Figure 3(a) shows the calculated band gaps and the absorption spectra based on GW quasiparticle calculations for alloys composition of $x = 0.25$ and $x = 0.50$. Note that the absorption coefficients α have been determined within the independent particle approximation and do not include excitonic effects, which typically increase α by about one order of magnitude in the vicinity of the band gap, e.g., in orth SnS.[9] While the Mg alloys exhibit a significant offset between the gap and the absorption onset, indicating an indirect character of the band gap, the Ca and Sr alloys behave instead like a direct gap semiconductor, where band gap and absorption onset coincide. Note, however, that since the crystal momentum is not a good quantum number in alloys, the direct/indirect character is only a qualitative measure. The actual observable of interest is the absorption strength as a function of the photon energy above the band gap. At a composition of $x = 0.25$, which roughly corresponds to the critical composition for the transition into the cubic rs structure, the band gap lies below that of orth SnS and increases up to 1.5 eV at $x = 0.50$. Thus, this composition range is predicted to cover the range of band gap energies that is most interesting for single-junction photovoltaics.

To elucidate the origin of the direct character and the magnitude of the band gaps, we show in Fig. 3(b) the calculated band structures of rs-SnS and CaS. In the cubic rs structure, SnS has an inverted band gap, a feature that has recently attracted much interest in the context of topological insulators.[31] Similar to the case of SnTe, which adopts rs as the ground state structure, the inversion occurs at the L point in the Brillouin zone.[32] The inverted band gap is small, 0.3 eV, with the valence band maximum (VBM) being at the L point, and the conduction band minimum (CBM) slightly off from the L point. CaS is a wide gap semiconductor with a calculated indirect gap of 5.2 eV, where the VBM is at the Γ and the CBM at the X point. When Ca is alloyed into rs

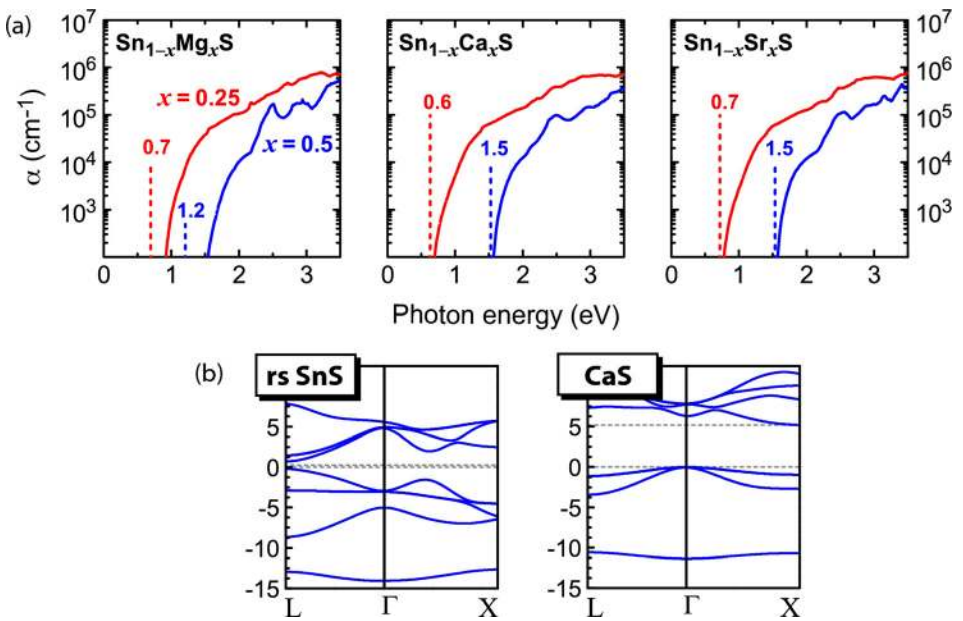

FIG. 3. (a) Calculated band gaps and optical absorption spectra of cubic SnS alloys for compositions $x = 0.25$ and 0.50. (b) Band structures of the cubic rs structure of the binary SnS and CaS compounds.

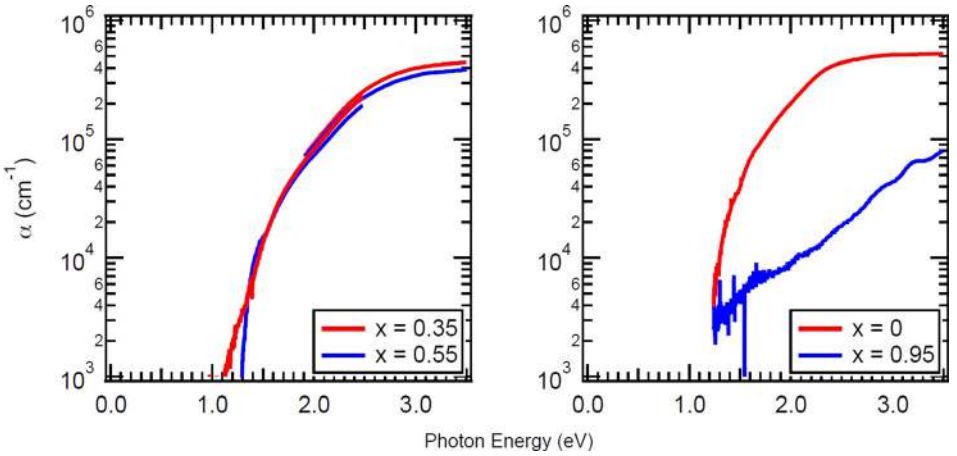

FIG. 4. Measured absorption spectra of $Sn_{1-x}Ca_xS$ thin films deposited on fused silica for (left panel) x = 0.35 or 0.55 and (right panel) x = 0 or 0.95.

SnS, one can expect that the inversion at the L point is reversed, leading to a situation similar to that of PbTe which is known as a semiconductor with a narrow direct band gap at the L point.[32] Thus, within the above mentioned limitation of the meaning of the crystal momentum in alloys, the $Sn_{1-x}Ca_xS$ and $Sn_{1-x}Sr_xS$ alloys can be viewed as having a direct gap at the L point, which supports strong optical absorption due to the different parities of the VBM (L_6^+; Sn-*s* like) and CBM (L_6^-; Sn-*p* like).

Figure 4(a) shows the results of optical measurements for films with moderate calcium content ($x = 0.35$–0.55), indicating that the optical band gap varies from 1.1 to 1.3 eV and increases with rising Ca content. The absorption onset is steeper for the higher Ca concentration, which is a trend that—although less pronounced—is also seen in the theoretical data (cf. Fig. 3). For comparison, Fig. 4(b) shows also the absorption spectrum of orth SnS with an optical band gap of 1.25 eV. The indirect band gap at 1.07 eV, which was determined from measurements on bulk samples,[13] is not visible in Fig. 4(b) because the respective indirect transitions with an absorption coefficient in the range of 1–100 cm^{-1} are too weak to be observable in a thin film. Figure 4(b) shows further the optical spectrum for a film with approximately 95% calcium on the cation site, exhibiting a very slow onset of absorption with no obvious band gap. At this composition, Sn acts as a metallic impurity in CaS and causes a low level of absorption at all energies. While the absorption onset in the films shows the trends with compositions predicted by the calculations, the overall absorption spectra are more similar than the calculations predict. One should keep in mind that the calculations still assume a somewhat idealized alloy model and do not include all phonon-, defect-, or disorder-induced effects present in experiment.

In addition to the optical characterization, we also performed electrical measurements. The present (SnCa)S films were too resistive to determine the carrier mobility via the Hall effect, but thermopower measurements indicate that the films are *p*-type, with a Seebeck coefficient of 900–1900 μV/K, for films with 35%–55% Ca cation content.

VI. CONCLUSIONS

The prediction, synthesis, and characterization of $Sn_{1-x}Ca_xS$ exemplify how the functional properties of photovoltaic materials could be modified by inducing structural modifications of the crystal structures in an alloying approach. Beyond the implication of this materials system as a potential thin-film solar cell absorber, the present work suggests a broader question: "Which desirable functional materials properties might be achieved or manipulated via structural transitions in polymorphic materials when modifying the composition by alloying?"

ACKNOWLEDGMENTS

Part of this work was supported by the US Department of Energy under contract No. DE-AC36-08GO28308 to NREL. J.V. and S.L. were supported by the Office of Energy Efficiency and Renewable Energy within the SunShot initiative. R.K. was supported by the Office of Science, Office of Basic Energy Sciences, within an Energy Frontier Research Center. J.F. and J.T. were supported by the National Science Foundation under DMR 1035513. The use of high performance computing resources of the National Energy Research Scientific Computing Center and of NREL's Computational Science Center are gratefully acknowledged. We acknowledge Peter Eschbach of the OSU Electron Microscopy facility for assistance with the TEM measurements, Jaeseok Heo for target preparation, Brady Gibbons and Douglas Keszler for use of their x-ray equipment, and OSU MASC for support of deposition facilities.

[1]V. Fthenakis, Renewable Sustainable Energy Rev. **13**, 2746 (2009).
[2]M. Green, Prog. Photovoltaics **14**, 383 (2006).
[3]A. Luque and S. Hegedus, *Handbook of Photovoltaics Science and Engineering* (Wiley-Blackwell, 2010).
[4]M. Green, Prog. Photovoltaics **17**, 347 (2009).
[5]C. Wadia, A. P. Alivisatos, and D. M. Kammen, Environ. Sci. Technol. **43**, 2072 (2009).
[6]T. K. Todorov, K. B. Reuter, and D. B. Mitzi, Adv. Energy Mater. **22**, E156 (2010).
[7]Y. Wu, C. Wadia, W. Ma, B. Sadtler, and A. P. Alivisatos, Nano Lett. **8**, 2551 (2008).
[8]M. Umehara, Y. Takeda, T. Motohiro, T. Sakai, H. Awano, and R. Maekawa, Appl. Phys. Express **6**, 045501 (2013).
[9]J. Vidal, S. Lany, M. d'Avezac, A. Zunger, A. Zakutayev, J. Francis, and J. Tate, Appl. Phys. Lett. **100**, 032104 (2012).
[10]P. Sinsermsuksakul, J. Heo, W. Noh, A. S. Hock, and R. G. Gordon, Adv. Energy Mater. **1**, 1116 (2011).
[11]P. Sinsermsuksakul, K. Hartman, S.-B. Kim, J. Heo, L. Sun, H. H. Park, R. Chakraborty, T. Buonassisi, and R. G. Gordon, Appl. Phys. Lett. **102**, 053901 (2013).

[12]L. A. Burton and A. Walsh, Appl. Phys. Lett. **102**, 132111 (2013).
[13]W. Albers, C. Haas, and F. van der Maesen, J. Phys. Chem. Solids **15**, 306 (1960).
[14]M. Cardona and F. H. Pollak, Phys. Rev. **142**, 530 (1966).
[15]S. Badachhape and A. Goswami, J. Phys. Soc. Jpn. **17**, 251–253 (1962).
[16]D. Avellaneda, M. T. S. Nair, and P. K. Nair, J. Electrochem. Soc. **155**, D517–D525 (2008).
[17]T. Chattopadhyay, J. Pannetier, and H. G. Von Schnering, J. Phys. Chem. Solids **47**, 879–885 (1986).
[18]A. N. Mariano and K. L. Chopra, Appl. Phys. Lett. **10**, 282–284 (1967).
[19]L. A. Burton and A. Walsh, J. Phys. Chem. C **116**, 24262 (2012).
[20]G. Kresse and D. Joubert, Phys. Rev. B **59**, 1758 (1999); M. Shishkin and G. Kresse, Phys. Rev. B **74**, 035101 (2006).
[21]L. Hedin, Phys. Rev. **139**, A796 (1965).
[22]A. Zunger, S. H. Wei, L. G. Ferreira, and J. E. Bernard, Phys. Rev. Lett. **65**, 353 (1990).
[23]S. H. Wei, L. G. Ferreira, J. E. Bernard, and A. Zunger, Phys. Rev. B **42**, 9622 (1990).
[24]S. Lany, Phys. Rev. B **87**, 085112 (2013).
[25]I. Ho and G. B. Stringfellow, Appl. Phys. Lett. **69**, 2701 (1996).
[26]J. Adhikari and D. A. Kofke, J. Appl. Phys. **95**, 4500 (2004).
[27]B. N. Pantha, J. Li, J. Y. Lin, and H. X. Jiang, Appl. Phys. Lett. **93**, 182107 (2008).
[28]J. Francis, "Growth and characterization of the p-type semiconductors SnS and BiCuOSe," Ph.D. dissertation (Oregon State University, 2013).
[29]H. Luo, R. G. Greene, K. Ghandehari, T. Li, and A. L. Ruoff, Phys. Rev. B **50**, 16232 (1994).
[30]B. F. Bilenkii, A. G. Mikolaichuk, and D. M. Freik, Phys. Status Solidi B **28**, K5 (1968).
[31]T. H. Hsieh, H. Lin, J. Liu, W. Duan, A. Bansil, and L. Fu, Nat. Commun. **3**, 982 (2012).
[32]J. O. Dimmock, I. Meingailis, and A. J. Strauss, Phys. Rev. Lett. **16**, 1193 (1966).